

Sourcerer: Sample-based Maximum Entropy Source Distribution Estimation

Julius Vetter ^{*1} Guy Moss ^{*1} Cornelius Schröder ¹ Richard Gao ¹ Jakob H. Macke ^{1,2}

Abstract

Scientific modeling applications often require estimating a distribution of parameters consistent with a dataset of observations—an inference task also known as source distribution estimation. This problem can be ill-posed, however, since many different source distributions might produce the same distribution of data-consistent simulations. To make a principled choice among many equally valid sources, we propose an approach which targets the maximum entropy distribution, i.e., prioritizes retaining as much uncertainty as possible. Our method is purely sample-based—leveraging the Sliced-Wasserstein distance to measure the discrepancy between the dataset and simulations—and thus suitable for simulators with intractable likelihoods. We benchmark our method on several tasks, and show that it can recover source distributions with substantially higher entropy without sacrificing the fidelity of the simulations. Finally, to demonstrate the utility of our approach, we infer source distributions for parameters of the Hodgkin-Huxley neuron model from experimental datasets with thousands of measurements. In summary, we propose a principled framework for inferring unique source distributions of scientific simulator parameters while retaining as much uncertainty as possible.

1. Introduction

In many scientific and engineering disciplines, mathematical and computational simulators are used to gain mechanistic insights. A common challenge is to identify parameter settings of such simulators that make their outputs compatible with a set of empirical observations. For example, by finding a distribution of parameters that, when passed through the

^{*}Equal contribution ¹Machine Learning in Science, University of Tübingen and Tübingen AI Center, Germany ²Max Planck Institute for Intelligent Systems, Department Empirical Inference, Tübingen, Germany. Correspondence to: Julius Vetter <julius.vetter@uni-tuebingen.de>, Guy Moss <guy.moss@uni-tuebingen.de>.

Preprint. Under Review.

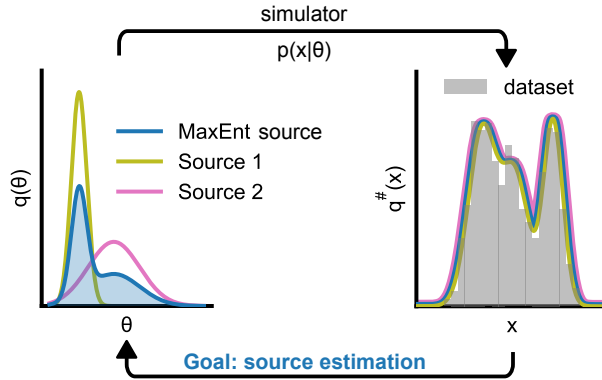


Figure 1. Maximum entropy source distribution estimation. Given an observed dataset $\mathcal{D} = \{x_1, \dots, x_n\}$ from some data distribution $p_o(x)$, the *source distribution estimation* problem is to find the parameter distribution $q(\theta)$ that reproduces $p_o(x)$ when passed through the simulator $p(x|\theta)$, i.e. $q^\#(x) = \int p(x|\theta)q(\theta)d\theta = p_o(x)$. This problem can be ill-posed, as there might be more than one distinct source distribution. We here target the source distribution with maximum entropy, which is unique.

simulator, produces a distribution of outputs that matches that of the empirical observations.

Suppose we have a stochastic simulator with input parameters θ and output x , which allows us to generate samples from the forward model $p(x|\theta)$ (which is usually intractable). We have acquired a dataset $\mathcal{D} = \{x_1, \dots, x_n\}$ of observations with empirical distribution $p_o(x)$, and want to identify a distribution $q(\theta)$ over parameters that, once passed through the simulator, yields a “pushforward” distribution of simulations $q^\#(x) = \int p(x|\theta)q(\theta)d\theta$ that is indistinguishable from the empirical distribution.

Our setting is known by different names in different disciplines, for example as *unfolding* in high energy physics (Cowan, 1998), *population of models* in electrophysiology (Lawson et al., 2018) and *population inference* in gravitational wave astronomy (Thrane & Talbot, 2019). Adopting the terminology of Vandegar et al. (2020), we refer to this task as *source distribution estimation*.

One approach to source distribution estimation is empirical Bayes (Robbins, 1956; Efron & Morris, 1972). Empirical Bayes uses hierarchical models in which each ob-

servation is modeled as arising from different parameters $p(x_i|\theta_i)$. The hyper-parameters of the prior (and thus the source q_ϕ) are found by optimizing the marginal likelihood $p(D) = \prod_i \int p(x_i|\theta)q_\phi(\theta)d\theta$ over ϕ . Empirical Bayes has been successfully applied to a range of applications (Lee & Mumford, 2003; Leng et al., 2013; Thrane & Talbot, 2019). However, the empirical Bayes approach is typically not applicable to models with intractable likelihoods, which is usually the case for scientific simulators. Using surrogate models for such likelihoods, empirical Bayes has been extended to increasingly more complicated parameterizations ϕ of the prior distribution, including neural networks (Wang et al., 2019; Vandegar et al., 2020).

A more general issue, however, is that the source distribution problem can often be ill-posed without the introduction of a hyper-prior or other regularization principles, as also noted in Vandegar et al. (2020): Distinct source distributions $q(\theta)$ can give rise to the same data distribution $q^\#(x)$ when pushed through the simulator $p(x|\theta)$ (Fig. 1, illustrative example in Appendix A.6.1).

We propose to resolve such ill-posedness by invoking the maximum entropy principle, i.e., to choose the “maximum ignorance” distribution within a class of valid distributions (Good, 1963; Jaynes, 1968). The maximum entropy principle has also been applied to specific source distribution estimation problems in scientific disciplines such as cosmology (Handley & Millea, 2018) and high-energy physics (Cowan, 1998). In practice, the maximum entropy distribution within some parametric family q_ϕ (e.g. a neural network) is found by finding the optimal ϕ^* .

Our contributions We here introduce *Sourcerer*¹: a general framework for source distribution estimation for simulators, providing two key innovations: First, we target the maximum entropy source distribution to obtain a well-posed problem, thereby increasing the entropy of the estimated source distributions at no cost to their fidelity. Second, we use general distance metrics between distributions such as the Sliced-Wasserstein distance, instead of maximizing the marginal likelihood as in empirical Bayes. This allows evaluation of the objective using *only samples*, removing the requirement to have simulators or surrogate models with a tractable likelihood. We validate our framework on multiple tasks, including tasks with high-dimensional observation space, which are challenging for likelihood-based methods. Finally, we apply our method to estimate the source distribution over the mechanistic parameters of the Hodgkin-Huxley model from a large (~ 1000 samples) dataset of electrophysiological recordings.

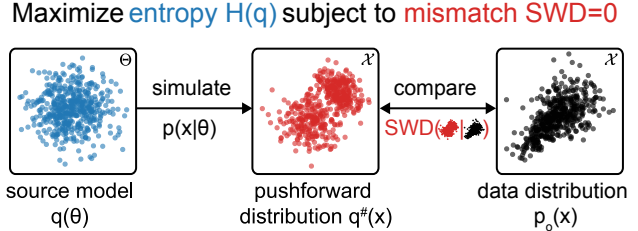


Figure 2. Overview of Sourcerer. Given a source distribution $q(\theta)$, we sample $\theta \sim q$ and simulate using $p(x|\theta)$ to obtain the pushforward distribution $q^\#(x) = \int p(x|\theta)q(\theta)d\theta$. We maximize the entropy of the source distribution $q(\theta)$ with a Sliced-Wasserstein distance (SWD) constraint between the pushforward of $q^\#$ and the data distribution $p_o(x)$. Θ and \mathcal{X} in top right corner of boxes denote parameter-space and data/observation-space, respectively.

2. Methods

We apply the principle of maximum entropy to solve the source distribution estimation problem. The (differential) entropy $H(p)$ of a distribution $p(\theta)$ is defined as

$$H(p) = - \int p(\theta) \log p(\theta) d\theta. \quad (1)$$

2.1. Data-consistency constraint

For a given distribution $q(\theta)$ and simulator with (possibly intractable) likelihood $p(x|\theta)$, we define the simulated *pushforward distribution* of $q(\theta)$ to be $q^\#(x) = \int_{\Theta} p(x|\theta)q(\theta)d\theta$. The maximum entropy source distribution is found by solving the constrained optimization problem

$$\begin{aligned} & \text{maximize} && H(q) \\ & \text{subject to} && \int p(x|\theta)q(\theta)d\theta = p_o(x). \end{aligned} \quad (2)$$

We show that, given that a source distribution exists, it is unique:

Proposition 2.1. *Let $Q \subset P(\Theta)$ be the set of source distributions q satisfying $q^\# = p_o$, where $P(\Theta)$ is the space of probability distributions on Θ . Suppose that Q is non-empty. Then the solution to Eq. (2) exists and is unique.*

Proof: see Appendix A.6.

In practice, the constraint in Eq. (2) can be formulated using any distance metric $D(\cdot, \cdot)$ on the space of probability distributions $P(\mathcal{X})$, as this constraint is satisfied if and only if $D(q^\#, p_o) = 0$.

A common approach to solve constrained optimization problems is the *penalty method* (Platt & Barr, 1987; Bertsekas

¹Code available at <https://github.com/mackelab/sourcerer>

& Rheinboldt, 2014). The penalty method removes the constraint, but modifies the objective function with a term that penalizes solutions which violate the constraint. This results in the unconstrained optimization problem

$$\text{maximize } \lambda H(q) - (1 - \lambda) \log(D(q^\#, p_o)^2), \quad (3)$$

where λ is a hyperparameter determining the strength of the penalty. The distance D is squared following the formulation of the penalty method, while the logarithm is introduced to improve numerical stability. We adopt a dynamic penalty scheme, where λ is initialized to one at the start of the search, and decreased as the search progresses to achieve better matching between $q^\#$ and p_o .

2.2. Reference distribution

For many tasks, there is an additional constraint in terms of a reference distribution $p(\theta)$. For example, in the Bayesian inference framework, it is common to have a prior distribution $p(\theta)$, encoding existing knowledge about the parameters θ from previous studies. In such cases, a distribution with higher entropy than $p(\theta)$, even if it is a valid source distribution, is not always desirable. We therefore adapt our objective function in Eq. (3) to minimize the Kullback-Leibler (KL) divergence between the source $q(\theta)$ and the reference $p(\theta)$:

$$\text{minimize } \lambda D_{KL}(q||p) + (1 - \lambda) \log(D(q^\#, p_o)^2). \quad (4)$$

The KL divergence term can be rewritten as $D_{KL}(q||p) = -H(q) + H(q, p)$, where $H(q, p) = -\int \log(p(\theta))q(\theta)d\theta$ is the cross-entropy between q and p . Thus, provided we can evaluate the density $p(\theta)$, we can obtain a sample-based estimate of the loss in Eq. (4). In our work, we consider $p(\theta)$ to be the uniform distribution over some bounded domain B_Θ (and hence the maximum entropy distribution on this domain). This ‘‘box prior’’ is often used as the naive estimate from literature observations in inference studies. More specifically, in this case, $H(q, p) = -1/|B_\Theta|$, where $|B_\Theta|$ is the volume of B_Θ . Therefore, it is independent of q , and hence minimizing the KL divergence is equivalent to maximizing $H(q)$. In the case where $p(\theta)$ is non-uniform (e.g., Gaussian) the cross-entropy term regularizes the loss by penalizing large $q(\theta)$ when $p(\theta)$ is small.

2.3. Sliced-Wasserstein as a distance metric

We are free to choose any distance metric $D(\cdot, \cdot)$ for the loss function Eq. (4). In particular, a *sample-based* metric is desirable, as it removes the requirement for the likelihood of the simulator $p(x|\theta)$ to be tractable. Thus, we can instead work with any differentiable simulator (or surrogate), which is usually an easier requirement to fulfill.

In this work, we use the Sliced-Wasserstein distance (SWD) (Bonneel et al., 2015; Kolouri et al., 2019; Nadjaifi et al.,

2020) of order 2. The SWD is defined as the expected value of the 1-dimensional Wasserstein distance between the projections of the distribution onto uniformly random directions u on the unit sphere \mathbb{S}^{d-1} in \mathbb{R}^d . More precisely, SWD is defined as

$$\text{SWD}_m(p, q) = \mathbb{E}_{u \sim \mathcal{U}(\mathbb{S}^{d-1})}[W_m(p_u, q_u)], \quad (5)$$

where p_u is the 1-dimensional distribution with samples $u^\top x$ for $x \sim p(x)$, and W_m is the 1-dimensional Wasserstein distance of order m . In the empirical setting where we are given n samples each from p_u and q_u respectively, the 1-dimensional Wasserstein distance is computed from the order statistics as

$$W_m(p_u, q_u) = \left(\sum_{i=1}^n \|x_p^{(i)} - x_q^{(i)}\|_m^m \right)^{1/m}, \quad (6)$$

where $x_p^{(i)}$ denotes the i -th order statistic of the samples from p_u (and similarly for $x_q^{(i)}$), and $\|\cdot\|_m$ denotes the L^m distance on \mathbb{R} . The sample-based 1-dimensional Wasserstein distance can thus be computed in $\mathcal{O}(n \log n)$ time in the number of datapoints n (Bonneel et al., 2015), which is significantly faster than computing the multi-dimensional Wasserstein distance ($\mathcal{O}(n^3)$, Kuhn, 1955). As the SWD is still a valid metric (Nadjaifi et al., 2020), it provides a fast and sample-based distance between any two potentially high-dimensional probability distributions.

2.4. Source Model

Our approach to source estimation only requires us to generate samples from our source, without estimating the likelihood of the resulting samples. In this work we use samplers as proposed in Vandegar et al. (2020) to parameterize a source model q_ϕ . Samplers employ unconstrained neural network architectures (in our case a multi-layer perceptron) to transform a random sample from $z \in \mathcal{N}(0, I)$ into a sample from q_ϕ . While samplers do not have a tractable likelihood, they are faster to evaluate than models with tractable likelihoods. Furthermore, by using unconstrained network architectures, samplers are flexible and additional constraints (e.g., symmetry, monotonicity) are easily introduced.

To use likelihood-free source parameterizations, we require a purely sample-based estimator for the entropy $H(q_\phi)$. This can be done using the Kozachenko-Leonenko entropy estimator (Kozachenko & Leonenko, 1987; Berrett et al., 2019), which is based on a nearest-neighbor density estimate. We use the Kozachenko-Leonenko estimator in this work for its simplicity, but note that sample-based entropy estimation is an active area of research, and other choices are possible (Pichler et al., 2022). Details in Appendix A.5.

2.5. Differentiable simulators and surrogates

One advantage of using the Sliced-Wasserstein distance for the constraint is that the likelihood $p(x|\theta)$ can be defined implicitly through a differentiable simulator, and does not need to be evaluated. For non-differentiable simulators with intractable likelihoods, a surrogate model can be trained before estimating the source. Similar to using sampler architectures for the source model, sample-based surrogates of $p(x|\theta)$ can be faster to train and evaluate. In our experiments, we compare the performance of sources learned with surrogates to the sources learned using the original simulator (when possible).

3. Experiments

First we evaluate our method on the three source estimation tasks presented in [Vandegar et al. \(2020\)](#). Since the Sliced-Wasserstein-based approach also works directly with differentiable simulators, we extend this benchmark with two high-dimensional tasks that involve differentiable simulators and which are widely used in other domains. Finally, we apply our method to a real-world dataset of electrophysiological recordings and a single-compartment Hodgkin-Huxley simulator.

3.1. Source Estimation Benchmark

Benchmark tasks The source estimation benchmark contains three simulators: two moons (TM), inverse kinematics (IK) and simple likelihood complex posterior (SLCP) (details about simulators and source distributions are in [Appendix A.1](#)). Notably, all three simulators are differentiable. Therefore, we can evaluate our method directly on the simulator as well as trained surrogates. For all three simulators, source estimation is performed on a synthetic dataset of 10000 observations that were generated by sampling from the original source distribution and evaluating the resulting pushforward distribution using the corresponding simulator. The quality of the estimated source distributions is measured using a classifier two sample test (C2ST) ([Lopez-Paz & Oquab, 2017](#)) between the observations and simulations from the source. If the estimated source is good, the simulations produced by that source should be indistinguishable from the original observations, that is, the classifier accuracy should be close to 50%. As a baseline, we compare to the log-marginal-likelihood (LML) estimator with 1024 Monte Carlo samples as described in [Vandegar et al. \(2020\)](#) (details in [Appendix A.4](#)).

Benchmark performance without entropy We first check whether minimizing the Sliced-Wasserstein distance, instead of maximizing the log-marginal likelihood, finds good source distributions without the entropy objective. We find that for the differentiable simulators, the Sliced-

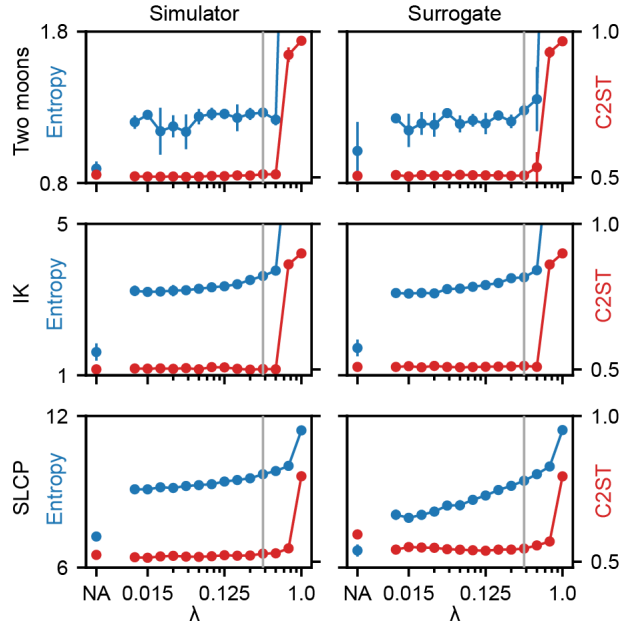


Figure 3. Results for the source estimation benchmark. Performance of our approach for all three benchmark tasks (Two moons, IK, SLCP) using both the original, differentiable simulators, and learned surrogates. Source estimation is performed without (NA) and with entropy maximization for different choices of λ . For all cases, mean C2ST accuracy between observations and simulations (lower is better) as well as the mean entropy of estimated sources (higher is better) over five runs are shown together with the standard deviation. The gray line at $\lambda = 0.35$ indicates our choice of λ for the numerical benchmark results (Table 1).

Wasserstein-based approach is able to find good source distributions with C2ST accuracies close to 50% for all benchmark tasks (Fig. 3, (NA)). This also applies when we use surrogate models to generate the pushforward distributions. In particular, the quality of the estimated source distributions matches those found by the LML estimator (Table 1).

Benchmark performance with entropy We now investigate the effect of estimating sources with the entropy objective as defined in Eq. (2). To this end, we evaluate the source for different levels of λ and a constant number of decay steps. More specifically, we sweep over λ with different powers of $2^{-\frac{1}{2}}$ from 2^0 to $2^{-\frac{14}{2}} \approx 0.008$. For the reported numerical results and figures, we pick a value of λ that results in a high entropy distribution and simulations that are in good agreement with the observations as measured by C2ST and SWD.

For all three benchmark simulators, the entropy of the estimated source can be drastically increased by using the entropy objective *without* any cost in the quality of sim-

Table 1. Numerical benchmark results for Sourcerer. We show the mean and standard deviation over 5 runs for differentiable simulators and surrogates of Sourcerer on the benchmark tasks, and compare to the log-marginal-likelihood (LML) estimator. All approaches achieve C2ST accuracies close to 50%. For the Sliced-Wasserstein-based approach, the entropies of the estimated sources are substantially higher (bold) with the entropy objective ($\lambda = 0.35$, gray line in Fig. 3). They are also higher than the entropy of the sources estimated by the baseline LML estimator.

Task	Two Moons		Inverse Kinematics		SLCP	
	C2ST acc.	Entropy	C2ST acc.	Entropy	C2ST acc.	Entropy
Sim. (w/o entropy)	0.51 (0.006)	0.9 (0.047)	0.5 (0.005)	1.61 (0.228)	0.52 (0.006)	7.23 (0.14)
Sim. (with entropy)	0.51 (0.005)	1.27 (0.025)	0.5 (0.002)	3.62 (0.031)	0.53 (0.003)	9.7 (0.03)
Sur. (w/o entropy)	0.5 (0.003)	1.01 (0.191)	0.51 (0.009)	1.72 (0.221)	0.59 (0.012)	6.68 (0.236)
Sur. (with entropy)	0.51 (0.002)	1.28 (0.046)	0.51 (0.003)	3.59 (0.071)	0.55 (0.004)	9.44 (0.019)
LML (only surrogate)	0.53 (0.005)	1.13 (0.093)	0.6 (0.014)	0.82 (0.712)	0.53 (0.006)	7.56 (0.097)

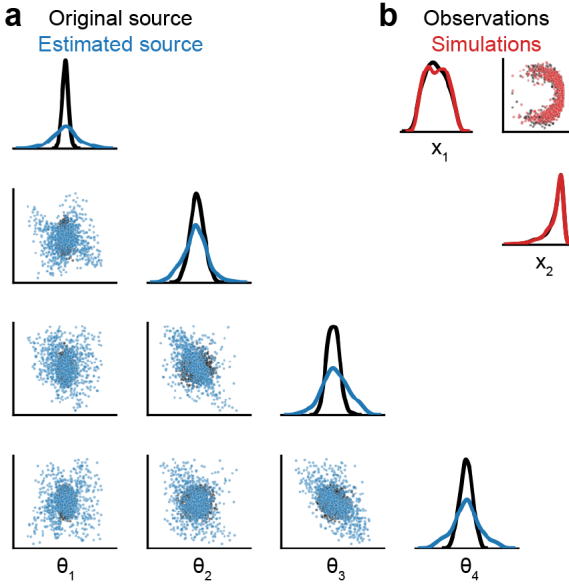


Figure 4. 1D and 2D marginal distributions for the IK task using the entropy objective (a) Original and estimated source estimated with the differentiable IK simulator ($\lambda = 0.35$). The estimated source has higher entropy than the original source that was used to generate the data. (b) Observations (simulated with parameters from the original source) and simulations (simulated with parameters from the estimated source) of the IK simulator.

ulations (Fig. 3). Despite maximizing the entropy, C2ST accuracy remains close to 50% across all benchmark tasks. Already for small values of λ , the entropy of estimated sources is substantially higher than that of sources estimated without the entropy objective. As expected, for large values of λ the SWD constraint becomes too weak, leading to a decrease in simulation fidelity. Empirically, we find this trade-off to be sharp: Below a critical value for λ , the estimated sources produce simulations that match the ob-

servations, but the fidelity of simulations rapidly declines once this critical λ value is surpassed. Furthermore, the entropy of source distributions estimated with the entropy objective are substantially larger than the ones estimated by the baseline LML estimator (Table 1).

In particular, for both IK and SLCP simulators, the entropy of the sources estimated by our method is higher than the entropy of the original source distribution (Fig. 4a and Appendix A.8) despite the simulations and observations being indistinguishable from each other (C2ST accuracy: 50%). This does not contradict our approach: The original source distribution just happens not to be the maximum entropy source for these simulators.

3.2. Differentiable Simulators: Lotka-Volterra and SIR

Since our method is sample-based and does not require likelihoods, it is possible to estimate sources by back-propagating through the differentiable simulators directly, instead of first training a surrogate likelihood model, which can be challenging when faced with high-dimensional data such as time series. Here, we highlight this capability by estimating source distributions for two high-dimensional simulators, the Lotka-Volterra model and the SIR (Susceptible, Infectious, Recovered) model. The Lotka-Volterra model is used to model the density of two populations, predators and prey. The SIR model is commonly used in epidemiology to model the spread of disease in a population (details about the SIR and Lotka-Volterra models and source distributions in Appendix A.1). Compared to the benchmark tasks in Sec. 3.1, the dimensionality of the data space is much larger: Both the Lotka-Volterra and the SIR model are simulated for 50 time points resulting in a 100 and 50 dimensional time series, respectively.

Furthermore, to show that unlike the LML estimator, our sample-based approach can deal with deterministic functions, we use a deterministic version of the SIR model with

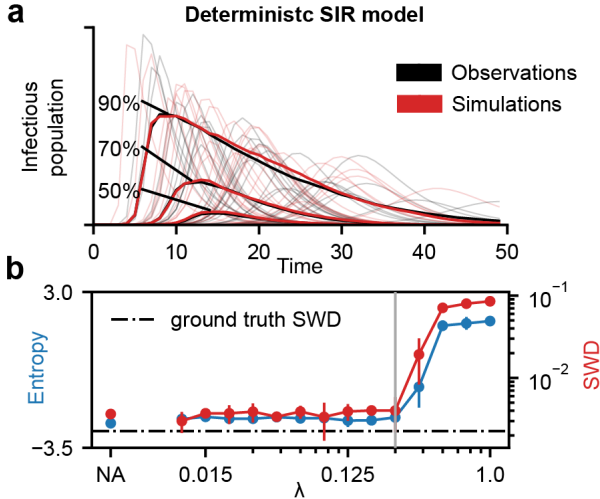


Figure 5. Source estimation on the deterministic SIR model.

(a) Percentile values of all samples computer per time point for simulations and observations ($\lambda = 0.25$). (b) Sliced-Wasserstein distance (lower is better) between observations and simulations as well as entropy of estimated sources (higher is better) for different choices of λ including $\lambda = 0.25$ (gray line) and without the entropy objective (NA). Mean and standard deviation over five runs are shown.

no observation noise. Similarly to the benchmark tasks, we define a source, and simulate 10000 observations using samples from this source to define a synthetic dataset on which to perform source distribution estimation. Here, we directly evaluate the quality of the estimated source distributions using the Sliced-Wasserstein distance (see Appendix A.8 for C2ST accuracies). We compare this distance to the expected ground truth distance between simulations of different sets of samples from the original source, which is the lowest distance possible.

Source estimation for the deterministic SIR model Our method is able to estimate a good source distribution for the deterministic SIR model: The Sliced-Wasserstein distance between simulations and observations is close to the expected ground truth distance (Fig. 5b). The percentiles between simulations and observations are in close agreement (Fig 5a). In contrast to the benchmark tasks, estimating sources with the entropy objective does not lead to an increase in entropy for the SIR model, and the quality of the estimated source remains constant for various choices of λ . A possible explanation for this is that there is no degeneracy in the parameter space of the deterministic simulator, and there exists only one valid source.

Source estimation on the probabilistic Lotka-Volterra model For the probabilistic Lotka-Volterra model, our method is also capable of estimating valid source distribu-

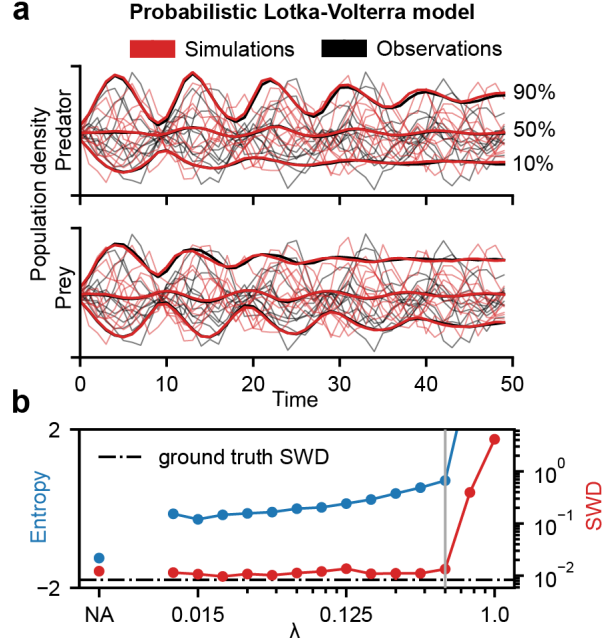


Figure 6. Source estimation for the probabilistic Lotka-Volterra model. (a) Percentile values of all samples computer per time point for simulations and observations ($\lambda = 0.5$). (b) Sliced-Wasserstein distance (lower is better) between observations and simulations as well as entropy of estimated sources (higher is better) for different choices of λ including $\lambda = 0.5$ (gray line) and the without the entropy objective (NA). Mean and standard deviation over five runs are shown.

tions. As for the SIR model, the Sliced-Wasserstein distance between simulations and observations is close to the expected ground truth distance (Fig. 6a), and simulations and observations are visually consistent (Fig. 6b). However, unlike the SIR model, estimating the source with the entropy objective yields a large increase in entropy compared to when not using the objective. For the Lotka-Volterra model, our method yields a substantially higher entropy at no additional cost in terms of source quality.

The experiments on the SIR and Lotka-Volterra models show that our approach is able to scale to higher dimensional problems and can use gradients of complex simulators to estimate source distributions directly from a set of observations.

3.3. Estimating source distributions for the single-compartment Hodgkin-Huxley model

Finally, we apply our model to a real-world dataset of electrophysiological recordings and the commonly used single compartment Hodgkin-Huxley simulator (Pospischil et al., 2008). The dataset (Scala et al., 2021) consists of 1033 electrophysiological recordings from the mouse motor cortex. In general, parameter inference for Hodgkin-Huxley models

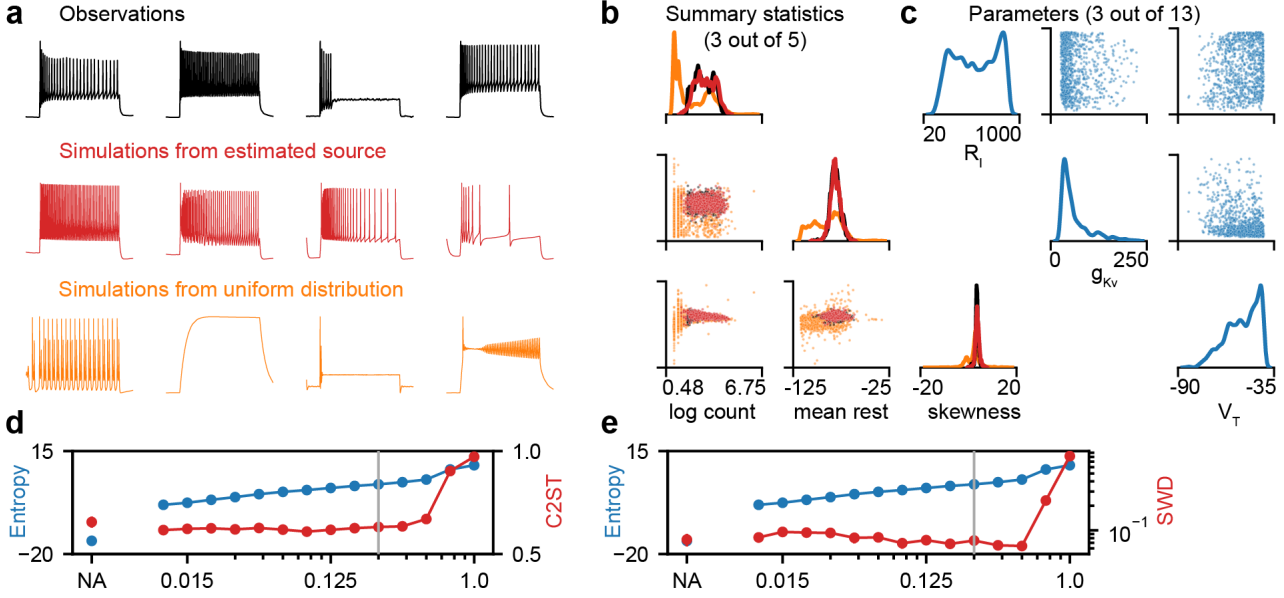


Figure 7. Source estimation for the single-compartment Hodgkin-Huxley model. (a) Example voltage traces of the real observations of the motor cortex dataset, simulations from the estimated source ($\lambda = 0.25$), and samples from the uniform distribution used to train the surrogate. (b) 1D and 2D marginals for three of the five summary statistics used to perform source estimation. (c) 1D and 2D marginal distributions of the estimated source for three of the 13 simulator parameters. (d and e) C2ST accuracy and Sliced-Wasserstein distance (lower is better) as well as entropy of estimated sources (higher is better) for different choices of λ including $\lambda = 0.25$ (gray line) and without the entropy objective (NA). Mean and standard deviation over five runs are shown.

can be challenging as models are often misspecified (Tolley et al., 2023; Bernaerts et al., 2023).

Single-compartment Hodgkin-Huxley simulator and summary statistics We use the simulator described in Bernaerts et al. (2023) with 13 parameters. In data space, we use 5 commonly used summary statistics of the observed and simulated spike trains. These are the (logged) number of spikes, the mean of the resting potential, and the mean, variance and skewness of the voltage during external current stimulation. As the internal noise in the simulator has little effect on the summary statistics, we train a simple multi-layer perceptron as surrogate on 10^6 simulations. The parameters used to generate these training simulations were sampled from a uniform distribution that was used as the prior in Bernaerts et al. (2023) (details on simulator, choice of surrogate and the surrogate training in Appendix A.7).

Source estimation As in all previous experiments, we perform several rounds of source estimation with different choices of λ and evaluate the quality of the simulations by visual inspection of example simulations, summary statistics, and C2ST accuracies.

The simulations look similar to the original recordings (all observations spike at least once, and so do all generated sim-

ulations) and show none of the unrealistic properties (e.g., spiking before the stimulus is applied) that can be observed in some of the box uniform prior simulations (Fig. 7a). This match is also confirmed by the distribution of summary statistics, which match closely between simulations and observations (Fig. 7b). Furthermore, our method achieves good C2ST accuracy of about 61% for different choices of λ (Fig. 7d), as well as a small Sliced-Wasserstein distance of 0.08 in the standardized space of summary statistics (Fig. 7e). While the source estimated without the entropy objective also achieves good fidelity, its entropy is significantly lower than any of the source distributions estimated with the entropy objective (Fig. 7d/e, example source distribution in Fig. 7c, full source in Appendix A.8).

Overall, these results demonstrate the importance of estimating source distributions using the entropy objective from Eq. (2), even on real-world datasets. Estimating the source distribution without the entropy objective can introduce severe bias, since the estimated source may ignore entire regions of the parameter space. In our particular example, the parameter space of the single-compartment Hodgkin-Huxley model is known to be highly degenerate, and a given observation can be generated by multiple parameter configurations (Edelman & Gally, 2001; Marder & Taylor, 2011).

4. Related Work

Neural Empirical Bayes High-dimensional source distributions have been estimated through variational approximations to the empirical Bayes problem. Louppe et al. (2019) trained a generative adversarial network (GAN) (Goodfellow et al., 2014) q_ψ to approximate the source. The use of a discriminator to compute an implicit distance makes this approach purely sample-based as well. In order to find the optimal ψ^* of the true data-generating process, they augmented the adversarial loss with a small entropy penalty on the source q_ψ . This penalty encourages low entropy, point mass distributions, which is the *opposite* of our approach. Vande-gar et al. (2020) take an empirical Bayes approach, and use normalizing flows for both the variational approximation of the source and as a surrogate for the likelihood $p(x|\theta)$. This allows for direct regression on the marginal likelihood, as all likelihoods can be computed directly. Finally, the empirical Bayes problem is also known as “unfolding” in the particle physics literature (Cowan, 1998), “population inference” in gravitational wave astronomy (Thrane & Talbot, 2019), and “population of models” in electrophysiology (Lawson et al., 2018). Approaches have been developed to identify the source distribution, including classical approaches that seek to increase the entropy of the learned sources (Reginatto et al., 2002).

Simulation-Based Inference The use of variational surrogates of the likelihood of a simulator with intractable likelihood is known as *Neural Likelihood Estimation* in the simulation-based inference (SBI) literature (Wood, 2010; Papamakarios et al., 2018; Lueckmann et al., 2019; Cranmer et al., 2019). In neural posterior estimation (Papamakarios & Murray, 2016; Lueckmann et al., 2017; Greenberg et al., 2019), an *amortized* posterior density estimate is learned, which can be applied to evaluate the posterior of a single observation $x_i \in \mathcal{D}$, if a prior distribution $p(\theta)$ is already known. An intuitive but incorrect approach to source distribution estimation would be to take the *average posterior* distribution over the observations \mathcal{D} ,

$$G_n(\theta) = \frac{1}{n} \sum_{i=1}^n p(\theta|x_i). \quad (7)$$

However, the average posterior does not always (and typically does not) converge to a source distribution in the infinite data limit, as shown for simple examples in Appendix A.6. Instead, SBI can be seen as a downstream task of source distribution estimation; once a prior has been learned from the dataset of observations with source estimation, the posterior can be estimated for each new observation individually.

Generalized Bayesian Inference Another related field is Generalized Bayesian Inference (GBI) (Bissiri et al., 2016;

Matsubara et al., 2022). Central to GBI is that in many inference applications, the exact Bayesian posterior distribution is not necessarily of interest, if one can find a distribution which can reproduce observations with high fidelity with respect to different distance metrics that can be chosen to target different features of the data. Similarly, Bayesian non-parametric methods (Orbanz & Teh, 2010; Lyddon et al., 2017; Dellaporta et al., 2022) learn a posterior directly on the data space which can then be used to sample from a posterior distribution over the parameter space.

5. Summary and Discussion

In this work, we introduced Sourcerer as a framework to estimate source distributions given datasets of observations. This is a common problem setting across a range of scientific and engineering disciplines. Our method has several advantages: first, we employ a maximum entropy approach, improving reproducibility of the learned source, as the maximum entropy source distribution is unique while the traditional source distribution estimation problem can be ill-posed. Second, our framework allows for sample-based optimization. In contrast to previous likelihood-based approaches, this scales more readily to higher dimensional problems, and can be applied to simulators without a tractable likelihood. We demonstrated the performance of our approach across a diverse suite of tasks, including deterministic and probabilistic simulators, low- and high-dimensional observation spaces, and a contemporary scientific task of estimating a source distribution for the single-compartment Hodgkin-Huxley model from a dataset of electrophysiological recordings. Throughout our experiments, we have consistently found that our approach yields higher entropy sources without reducing the fidelity of simulations from the learned source.

Limitations A limitation of this work is the penalty method approximation to the constrained optimization problem. The penalty method leads to a more tractable unconstrained optimization problem, but solutions are not guaranteed to satisfy the constraints exactly as a result. The use of more sophisticated methods to solve this constrained optimization problem can address this limitation (Gill et al., 2019; Chong et al., 2023). Additionally, we used the Sliced-Wasserstein distance as the constraint for source distributions in this work. In practice, different distance metrics can lead to different sources, depending on its sensitivity to different features. While our method is compatible with any sample-based differentiable distance metric between two distributions, there is still an onus on the practitioner to carefully select a reasonable distance metric for the data at hand. Similarly, there is a dependence on the hyperparameter λ , though as we demonstrate, our results are robust to a large range of λ . Finally, the method requires a differentiable

simulator, which in practice may require the training of a surrogate model. While this is a common requirement for simulation-based methods, this could present a challenge for some applications.

6. Ethics Statement

We used data recorded from animal experiments in the mouse. The data we used were recorded for an independent study and have recently been made publicly available (Scala et al., 2021). While our work has the potential to aid in scientific discovery across a broad range of disciplines, one could also imagine undesired uses.

Acknowledgements

This work was funded by the German Research Foundation (DFG) under Germany’s Excellence Strategy – EXC number 2064/1 – 390727645 and SFB 1233 ‘Robust Vision’ (276693517). This work was co-funded by the German Federal Ministry of Education and Research (BMBF): Tübingen AI Center, FKZ: 01IS18039A and the European Union (ERC, DeepCoMechTome, 101089288). Views and opinions expressed are however those of the author(s) only and do not necessarily reflect those of the European Union or the European Research Council. Neither the European Union nor the granting authority can be held responsible for them. JV is supported by the AI4Med-BW graduate program. JV and GM are members of the International Max Planck Research School for Intelligent Systems (IMPRS-IS). We would like to thank Jonas Beck, Sebastian Bischoff, Michael Deistler, Manuel Glöckler, Jaivardhan Kapoor, Auguste Schulz, and all members of Mackelab for feedback and discussion throughout the project.

References

Bernaerts, Y., Deistler, M., Goncalves, P. J., Beck, J., Stimpert, M., Scala, F., Tolias, A. S., Macke, J. H., Kobak, D., and Berens, P. Combined statistical-mechanistic modeling links ion channel genes to physiology of cortical neuron types. *bioRxiv*, 2023.

Berrett, T. B., Samworth, R. J., and Yuan, M. Efficient multivariate entropy estimation via k -nearest neighbour distances. *The Annals of Statistics*, 2019.

Bertsekas, D. and Rheinboldt, W. *Constrained Optimization and Lagrange Multiplier Methods*. Computer science and applied mathematics. Elsevier Science, 2014.

Bissiri, P. G., Holmes, C. C., and Walker, S. G. A general framework for updating belief distributions. *Journal of the Royal Statistical Society Series B: Statistical Methodology*, 2016.

Bonneel, N., Rabin, J., Peyré, G., and Pfister, H. Sliced and Radon Wasserstein barycenters of measures. *Journal of Mathematical Imaging and Vision*, 2015.

Chong, E., Lu, W., and Zak, S. *An Introduction to Optimization: With Applications to Machine Learning*. Wiley, 2023.

Cowan, G. *Statistical Data Analysis*. Oxford science publications. Clarendon Press, 1998.

Cranmer, K., Brehmer, J., and Louppe, G. The frontier of simulation-based inference. *Proceedings of the National Academy of Sciences*, 2019.

DellaPorta, C., Knoblauch, J., Damoulas, T., and Briol, F.-X. Robust Bayesian inference for simulator-based models via the MMD posterior bootstrap. In *International Conference on Artificial Intelligence and Statistics*. PMLR, 2022.

Dinh, L., Sohl-Dickstein, J., and Bengio, S. Density estimation using Real NVP. In *International Conference on Learning Representations*, 2017.

Edelman, G. M. and Gally, J. A. Degeneracy and complexity in biological systems. *Proceedings of the National Academy of Sciences*, 2001.

Efron, B. and Morris, C. Limiting the risk of Bayes and empirical Bayes estimators, part ii: The empirical Bayes case. *Journal of the American Statistical Association*, 1972.

Gill, P. E., Murray, W., and Wright, M. H. *Practical Optimization*. Society for Industrial and Applied Mathematics, 2019.

Glöckler, M., Deistler, M., and Macke, J. H. Adversarial robustness of amortized Bayesian inference. In *International Conference on Machine Learning*, 2023.

Gonçalves, P. J., Lueckmann, J.-M., Deistler, M., Nonnenmacher, M., Öcal, K., Bassetto, G., Chintaluri, C., Podlaski, W. F., Haddad, S. A., Vogels, T. P., et al. Training deep neural density estimators to identify mechanistic models of neural dynamics. *Elife*, 2020.

Good, I. J. Maximum entropy for hypothesis formulation, especially for multidimensional contingency tables. *Annals of Mathematical Statistics*, 1963.

Goodfellow, I., Pouget-Abadie, J., Mirza, M., Xu, B., Warde-Farley, D., Ozair, S., Courville, A., and Bengio, Y. Generative adversarial nets. In *Advances in Neural Information Processing Systems*, 2014.

Greenberg, D. S., Nonnenmacher, M., and Macke, J. H. Automatic posterior transformation for likelihood-free inference. In *International Conference on Machine Learning*, 2019.

Handley, W. and Millea, M. Maximum-entropy priors with derived parameters in a specified distribution. *Entropy*, 2018.

Jaynes, E. T. Prior probabilities. *IEEE Transactions on Systems Science and Cybernetics*, 1968.

Kingma, D. P. and Ba, J. Adam: A method for stochastic optimization. *arXiv preprint arXiv:1412.6980*, 2014.

Kolouri, S., Nadjahi, K., Simsekli, U., Badeau, R., and Rohde, G. Generalized Sliced Wasserstein distances. In *Advances in Neural Information Processing Systems*, 2019.

Kozachenko, L. and Leonenko, N. A statistical estimate for the entropy of a random vector. *Problems of Information Transmission*, 1987.

Kuhn, H. W. The Hungarian method for the assignment problem. *Naval Research Logistics Quarterly*, 1955.

Lawson, B. A. J., Drovandi, C. C., Cusimano, N., Burrage, P., Rodriguez, B., and Burrage, K. Unlocking data sets by calibrating populations of models to data density: A study in atrial electrophysiology. *Science Advances*, 2018.

Lee, T. S. and Mumford, D. Hierarchical Bayesian inference in the visual cortex. *J. Opt. Soc. Am. A*, 2003.

Leng, N., Dawson, J. A., Thomson, J. A., Ruotti, V., Rissman, A. I., Smits, B. M. G., Haag, J. D., Gould, M. N., Stewart, R. M., and Kendziorski, C. EBSeq: an empirical bayes hierarchical model for inference in RNA-seq experiments. *Bioinformatics*, 2013.

Lopez-Paz, D. and Oquab, M. Revisiting classifier two-sample tests. In *International Conference on Learning Representations*, 2017.

Louppe, G., Hermans, J., and Cranmer, K. Adversarial variational optimization of non-differentiable simulators. In Chaudhuri, K. and Sugiyama, M. (eds.), *International Conference on Artificial Intelligence and Statistics*, Proceedings of Machine Learning Research, 2019.

Lueckmann, J.-M., Goncalves, P. J., Bassetto, G., Öcal, K., Nonnenmacher, M., and Macke, J. H. Flexible statistical inference for mechanistic models of neural dynamics. In *Advances in Neural Information Processing Systems*, 2017.

Lueckmann, J.-M., Bassetto, G., Karaletsos, T., and Macke, J. H. Likelihood-free inference with emulator networks. In *Proceedings of The 1st Symposium on Advances in Approximate Bayesian Inference*, Proceedings of Machine Learning Research, 2019.

Lueckmann, J.-M., Boelts, J., Greenberg, D., Goncalves, P., and Macke, J. Benchmarking simulation-based inference. In *International Conference on Artificial Intelligence and Statistics*, 2021.

Lyddon, S., Holmes, C. C., and Walker, S. G. General Bayesian updating and the loss-likelihood bootstrap. *Biometrika*, 2017.

Marder, E. and Taylor, A. L. Multiple models to capture the variability in biological neurons and networks. *Nature neuroscience*, 2011.

Matsubara, T., Knoblauch, J., Briol, F.-X., and Oates, C. J. Robust generalised Bayesian inference for intractable likelihoods. *Journal of the Royal Statistical Society Series B: Statistical Methodology*, 2022.

Nadjahi, K., Durmus, A., Chizat, L., Kolouri, S., Shahrami-pour, S., and Simsekli, U. Statistical and topological properties of sliced probability divergences. In *Advances in Neural Information Processing Systems*, 2020.

Orbánz, P. and Teh, Y. W. Bayesian nonparametric models. *Encyclopedia of Machine Learning*, 2010.

Papamakarios, G. and Murray, I. Fast ϵ -free inference of simulation models with Bayesian conditional density estimation. In *Advances in Neural Information Processing Systems*, 2016.

Papamakarios, G., Sterratt, D. C., and Murray, I. Sequential neural likelihood: Fast likelihood-free inference with autoregressive flows. In *International Conference on Artificial Intelligence and Statistics*, 2018.

Pichler, G., Colombo, P., Boudiaf, M., Koliander, G., and Piantanida, P. A differential entropy estimator for training neural networks. In *International Conference on Machine Learning*, 2022.

Platt, J. and Barr, A. Constrained differential optimization. In *Neural Information Processing Systems*, 1987.

Pospischil, M., Toledo-Rodriguez, M., Monier, C., Piwkowska, Z., Bal, T., Frégnac, Y., Markram, H., and Destexhe, A. Minimal Hodgkin–Huxley type models for different classes of cortical and thalamic neurons. *Biological cybernetics*, 2008.

Reginatto, M., Goldhagen, P., and Neumann, S. Spectrum unfolding, sensitivity analysis and propagation of uncertainties with the maximum entropy deconvolution code

MAXED. *Nuclear Instruments and Methods in Physics Research Section A: Accelerators, Spectrometers, Detectors and Associated Equipment*, 2002.

Robbins, H. E. An empirical bayes approach to statistics. In *Breakthroughs in Statistics: Foundations and basic theory*, 1956.

Scala, F., Kobak, D., Bernabucci, M., Bernaerts, Y., Cadwell, C. R., Castro, J. R., Hartmanis, L., Jiang, X., Latus, S., Miranda, E., et al. Phenotypic variation of transcriptomic cell types in mouse motor cortex. *Nature*, 2021.

Thrane, E. and Talbot, C. An introduction to Bayesian inference in gravitational-wave astronomy: Parameter estimation, model selection, and hierarchical models. *Publications of the Astronomical Society of Australia*, 2019.

Tolley, N., Rodrigues, P. L., Gramfort, A., and Jones, S. Methods and considerations for estimating parameters in biophysically detailed neural models with simulation based inference. *bioRxiv*, 2023.

Vaidya, P. M. Ano(n logn) algorithm for the all-nearest-neighbors problem. *Discrete & Computational Geometry*, 1989.

Vandegar, M., Kagan, M., Wehenkel, A., and Louppe, G. Neural empirical Bayes: Source distribution estimation and its applications to simulation-based inference. In *International Conference on Artificial Intelligence and Statistics*, 2020.

Wang, Y., Miller, A. C., and Blei, D. M. Comment: Variational Autoencoders as Empirical Bayes. *Statistical Science*, 2019.

Wood, S. N. Statistical inference for noisy nonlinear ecological dynamic systems. *Nature*, 2010.

A. Appendix

A.1. Simulators and sources

Here we provide a definition of the three benchmark tasks Two Moons (TM), Inverse Kinematics (IK) and Simple Likelihood Complex Posterior (SLCP) as well as the two high-dimensional simulators, the SIR and Lotka-Volterra model. We also describe the original source distribution used to generate the synthetic observations, and the bounds of the reference uniform distribution on the parameters.

A.1.1. TWO MOONS SIMULATOR

Dimensionality	$x \in \mathbb{R}^2, \theta \in \mathbb{R}^2$
Bounding domain	$[-5, 5]^2$
Original source	$\theta \sim \mathcal{U}([-1, 1]^2)$
Simulator	$x \theta = \begin{bmatrix} r \cos(\alpha) + 0.25 \\ r \sin(\alpha) \end{bmatrix} + \begin{bmatrix} - \theta_1 + \theta_2 /\sqrt{2} \\ (-\theta_1 + \theta_2)/\sqrt{2} \end{bmatrix}$, where $\alpha \sim U(-\pi/2, \pi/2)$, $r \sim \mathcal{N}(0.1, 0.01^2)$.
References	Vandegar et al. (2020) ; Lueckmann et al. (2021)

A.1.2. INVERSE KINEMATICS SIMULATOR

Dimensionality	$x \in \mathbb{R}^2, \theta \in \mathbb{R}^4$
Bounding domain	$[-\pi, \pi]^4$
Original source	$\theta \sim \mathcal{N}(0, \text{Diag}(\frac{1}{2}, \frac{1}{4}, \frac{1}{4}, \frac{1}{4}))$
Simulator	$x_1 = \theta_1 + l_1 \sin(\theta_2 + \epsilon) + l_2 \sin(\theta_2 + \theta_3 + \epsilon) + l_3 \sin(\theta_2 + \theta_3 + \theta_4 + \epsilon)$, $x_2 = l_1 \cos(\theta_2 + \epsilon) + l_2 \cos(\theta_2 + \theta_3 + \epsilon) + l_3 \cos(\theta_2 + \theta_3 + \theta_4 + \epsilon)$, where $l_1 = l_2 = 0.5$, $l_3 = 1.0$ and $\epsilon \sim \mathcal{N}(0, 0.00017^2)$ is a small noise term.
References	Vandegar et al. (2020)

A.1.3. SLCP SIMULATOR

Dimensionality	$x \in \mathbb{R}^8, \theta \in \mathbb{R}^5$
Bounding domain	$[-5, 5]^5$
Original source	$\theta \sim \mathcal{U}([-3, 3]^5)$
Simulator	$x \theta = (x_1, \dots, x_4)$, $x_i \sim \mathcal{N}(m_\theta, S_\theta)$, where $m_\theta = \begin{bmatrix} \theta_1 \\ \theta_2 \end{bmatrix}$, $S_\theta = \begin{bmatrix} s_1^2 & \rho s_1 s_2 \\ \rho s_1 s_2 & s_2^2 \end{bmatrix}$, $s_1 = \theta_3^2$, $s_2 = \theta_4^2$, $\rho = \tanh \theta_5$
References	Vandegar et al. (2020) ; Lueckmann et al. (2021)

A.1.4. SIR MODEL

Dimensionality	$x \in \mathbb{R}^{50}, \theta \in \mathbb{R}^2$
Bounding domain	$[0.001, 3]^2$
Original source	$\beta \sim \text{LogNormal}(\log(0.4), 0.5)$ $\gamma \sim \text{LogNormal}(\log(0.125), 0.2)$
Simulator	$x \theta = (x_1, \dots, x_{50})$, where $x_i = I_i/N$ equally spaced and I is simulated from $\frac{dS}{dt} = -\beta \frac{SI}{N}$, $\frac{dI}{dt} = \beta \frac{SI}{N} - \gamma I$, $\frac{dR}{dt} = \gamma I$ with initial values $S = N - 1$, $I = 1$, $R = 0$ and $N = 10^6$.
References	Lueckmann et al. (2021)

A.1.5. LOTKA-VOLTERRA MODEL

Dimensionality	$x \in \mathbb{R}^{100}, \theta \in \mathbb{R}^4$
Bounding domain	$[0.1, 3]^4$
Original source	$\theta' \sim \mathcal{N}(0, 0.5^2)^4$, pushed through $\theta = f(\theta') = \exp(\sigma(\theta'))$, where σ is the sigmoid function.
Simulator	$x \theta = (x_1^X, \dots, x_{50}^X, x_1^Y, \dots, x_{50}^Y)$, where $x_i^X \sim \mathcal{N}(X, 0.05^2)$, $x_i^Y \sim \mathcal{N}(Y, 0.05^2)$ equally spaced, and X, Y are simulated from $\frac{dX}{dt} = \alpha X - \beta XY$, $\frac{dY}{dt} = -\gamma Y + \delta XY$ with initial values $X = Y = 1$.
References	Glöckler et al. (2023)

A.2. Source model

Throughout all our experiments, we use samplers as the source models. The sampler architecture is a three-layer multi-layer perceptron with dimension of 100, ReLU activations and batch normalization as our source model. Samples are generated by drawing a sample $s \sim \mathcal{N}(0, I)$ from the standard multivariate Gaussian and then (non-linearly) transforming s with the neural network.

A.3. Surrogates for the benchmark tasks

We follow [Vandegar et al. \(2020\)](#) and train RealNVP flows ([Dinh et al., 2017](#)) as surrogates for the three benchmark tasks. For all benchmark tasks, the RealNVP surrogates have a flow length of 8 layers with a hidden dimension of 50.

Surrogates were trained using the Adam optimizer ([Kingma & Ba, 2014](#)) on 15000 samples and simulator evaluations from the uniform distribution over the bounding domain (learning rate 10^{-4} , weight decay $5 \cdot 10^{-5}$, training batch size 256). In addition, 20% of the data was used for validation.

A.4. Details on source estimation

For both the benchmark tasks and high dimensional simulators, sources were estimated from 10000 synthetic observations that were generated by simulating samples from an original previously defined source.

For the benchmark tasks, we used 500 linear decay steps to the specified λ and optimized the source model using the Adam optimizer with a learning rate of 10^{-4} and weight decay of 10^{-5} . The two high dimensional simulators were optimized with a higher learning rate of 10^{-3} and 50 linear decay steps. In both cases, early stopping was performed when the overall loss in Eq. (4) did not improve over a set number of training iterations.

As a baseline, we use the log-marginal-likelihood (LML) estimator as described in [Vandegar et al. \(2020\)](#). Specifically, we use the biased estimator with 1024 samples per observation (\mathcal{L}_{1024}), which are used to compute the Monte Carlo integral. Unlike our Sliced-Wasserstein-based approach, the LML estimator does not operate on the whole dataset of observations directly but attempts to maximize the marginal likelihood per observation and thus uses part of the observations as a validation set. To ensure a fair comparison, we increased the number of observations to 11112 for all LML estimator experiments, which results in a training dataset of 10000 observations when using 10% as a validation set. For training, we again used the Adam optimizer (learning rate 10^{-4} , weight decay 10^{-5} , training batch size 128).

A.5. Kozachenko-Leonenko entropy estimators

Our use of samplers requires us to use a sample-based estimate of (differential) entropy, since no tractable likelihood is available (see Sec. 2.4).

We use the Kozachenko-Leonenko estimator ([Kozachenko & Leonenko, 1987](#); [Berrett et al., 2019](#)) for a set of samples $\{\theta_i\}_{i=1}^n$ from a distribution $p(\theta) \in P(\Theta)$, given by

$$H(q_\phi) \approx \frac{d}{m} \left[\sum_{i=1}^n \log(d_i) \right] - g(k) + g(n) + \log(V_d), \quad (8)$$

where d_i is the distance of θ_i from its k -th nearest neighbor in $\{\theta_j\}_{j \neq i}$, d is the dimensionality of Θ , m is the number of non-zero values of d_i , g is the digamma function, and V_d is the volume of the unit ball using the same distance measure as used to compute the distances d_i .

The Kozachenko-Leonenko estimator is differentiable and can be used for gradient-based optimization. The all-pairs nearest neighbor problem can be efficiently solved in $\mathcal{O}(n \log n)$ ([Vaidya, 1989](#)). In practice, we find all nearest neighbors by computing all pairwise distances on a fixed number of samples. Throughout all experiments, 512 source distribution samples were used to estimate the entropy during training.

A.6. Mathematical details

A.6.1. UNIQUENESS OF MAXIMUM ENTROPY SOURCE DISTRIBUTION

Here, we prove the uniqueness of the maximum entropy source distribution (Proposition 2.1). First, however, we demonstrate for a simple example that the source distribution without the maximum entropy condition is not unique.

Example of non-uniqueness Consider the (deterministic) simulator $x = f(\theta) = |\theta|$. Further assume that our observed distribution is the uniform distribution $p(x) = \mathcal{U}(x; a, b)$, where $0 < a < b$. Due the symmetry of f , the source distribution $p(\theta)$ for the observed distribution $p(x)$ is not unique. Any convex combination of form $\alpha u_1(\theta) + (1 - \alpha)u_2$, where $u_1(\theta) = \mathcal{U}(\theta; -b, -a)$ and $u_2(\theta) = \mathcal{U}(\theta; a, b)$ and $\alpha \in [0, 1]$ provides a valid source distribution. The maximum entropy source distribution is unique and is attained if both distributions are weighted equally with $\alpha = 0.5$.

Proof of Proposition 2.1 We require two results to prove that the maximum entropy source distribution is unique. First, the set of source distributions Q is a convex set, i.e., convex combinations of source distributions are also source distributions. Second, entropy is strictly concave.

Let q_1 and q_2 be two distinct source distributions, then their convex combination $q = \alpha q_1 + (1 - \alpha)q_2$, $\alpha \in [0, 1]$ is a valid probability distribution supported on both of the supports of q_1 and q_2 .

Sources distributions are closed under convex combination: q is also a source distribution, since

$$\begin{aligned} q^\#(x) &= \int p(x|\theta) \cdot (\alpha q_1(\theta) + (1 - \alpha)q_2(\theta)) d\theta \\ &= \alpha \int p(x|\theta) q_1(\theta) d\theta + (1 - \alpha) \int p(x|\theta) q_2(\theta) d\theta \\ &= \alpha p_o(x) + (1 - \alpha)p_o(x) = p_o(x). \end{aligned} \tag{9}$$

Entropy is (strictly) concave: the entropy of q satisfies

$$\begin{aligned} H(q) &= - \int (\alpha q_1(\theta) + (1 - \alpha)q_2(\theta)) \cdot \log(\alpha q_1(\theta) + (1 - \alpha)q_2(\theta)) d\theta \\ &\geq - \int [\alpha q_1(\theta) \log(q_1(\theta)) + (1 - \alpha)q_2(\theta) \log(q_2(\theta))] d\theta \\ &= \alpha H(q_1) + (1 - \alpha)H(q_2), \end{aligned} \tag{10}$$

where we used the fact that the function $f(x) = x \log x$ is convex on $[0, \infty)$, and hence $-f$ is concave. Furthermore, $f(x)$ is strictly convex on $[0, \infty)$, so for any $\theta \in \Theta$, the equality of the integrands

$$\alpha q_1(\theta) + (1 - \alpha)q_2(\theta) \log(\alpha q_1(\theta) + (1 - \alpha)q_2(\theta)) = \alpha q_1(\theta) \log(q_1(\theta)) + (1 - \alpha)q_2(\theta) \log(q_2(\theta)) \tag{11}$$

holds if and only if $\alpha \in \{0, 1\}$ or $q_1(\theta) = q_2(\theta)$. Since q_1 and q_2 are assumed distinct, that is, it holds $q_1(\theta) \neq q_2(\theta)$ on a positive measure set, the integral equality in Eq. (10) only holds if $\alpha \in \{0, 1\}$, and thus entropy is strictly concave.

The proof of uniqueness then follows by contradiction. Suppose there exist two distinct maximum entropy source distributions, q_1^* and q_2^* . Then their average, $0.5(q_1^* + q_2^*)$ is still a source distribution, and has higher entropy, contradicting our assumptions on q_1^* and q_2^* .

A.6.2. EXAMPLES RELATED TO THE AVERAGE POSTERIOR DISTRIBUTION

In general, the average posterior distribution is not a valid source distribution. The average posterior distribution is defined in Eq. (7). The infinite data limit is given by $G_n(\theta) \xrightarrow{n \rightarrow \infty} G(\theta) = \int p(\theta|x)p_o(x)dx$. Here, we provide two examples, one based on coin flips, and one based on Gaussian distributions to illustrate this point.

Coin-flip example Consider the classical coin flip example, where the probability of heads (H) follows a Bernoulli distribution with parameter θ . The source distribution estimation problem for this setting would consist of the outcomes of flipping n distinct coins, with potentially different values θ_i .

Proposition A.1. Suppose we have a Beta prior distribution on the Bernoulli parameter $\theta \sim \text{Beta}(\alpha, \beta)$ with parameters $\alpha = \beta = 1$, and that the empirical measurements consist of 70% heads, i.e.:

$$p_o(x) = \begin{cases} 0.7 & x = H \\ 0.3 & x = T \end{cases}$$

Then the average posterior $G(\theta) = \int p(\theta|x)p_o(x)dx$ is not a valid source distribution for $p_o(x)$.

Proof: Since the Beta distribution is the conjugate prior for the Bernoulli likelihood, the single-observation posteriors are known to be $p(\theta|x = H) = \text{Beta}(2, 1)$ and $p(\theta|x = T) = \text{Beta}(1, 2)$. Hence, the average posterior is

$$G(\theta) = 0.3 \cdot \text{Beta}(1, 2) + 0.7 \cdot \text{Beta}(2, 1). \quad (12)$$

However, the ratio of heads observed when pushing this distribution through the Bernoulli simulator is

$$\begin{aligned} G^\#(x = H) &= \int_0^1 \theta [0.3 \cdot \text{Beta}(\theta; 1, 2) + 0.7 \cdot \text{Beta}(\theta; 2, 1)] d\theta \\ &= \int_0^1 \theta \left[0.3 \frac{1-\theta}{B(1, 2)} + 0.7 \frac{\theta}{B(2, 1)} \right] d\theta \\ &= 2 \int_0^1 [0.3\theta(1-\theta) + 0.7\theta^2] d\theta \\ &= 0.3\theta^2 + \frac{2}{3}0.4\theta^3 \Big|_0^1 \\ &\approx 0.567 \neq 0.7, \end{aligned} \quad (13)$$

where we have used the fact that the Beta function takes the values $B(1, 2) = B(2, 1) = 1/2$. Therefore, the pushforward of the average posterior distribution does not recover the correct ratio of heads, and so it is not a valid source distribution.

Gaussian example The average posterior distribution is also not always a valid source distribution in the continuous case, and we show this for a simple univariate Gaussian simulator with $x, \theta \in \mathbb{R}$.

Proposition A.2. Suppose we are given a Gaussian likelihood $p(x|\theta) = \mathcal{N}(x; \theta, 1^2)$, and a data distribution $p_o(x) = \mathcal{N}(x; 0, \sigma_D^2)$. Then for any Gaussian prior $p(\theta) = \mathcal{N}(\theta; 0, \sigma^2)$, the limit of the average posterior distribution, $G_n(\theta)$ as $n \rightarrow \infty$ is not a valid source distribution for $p_o(x)$.

Proof: The proof follows from the application of the well-known formulae for Gaussian posterior and marginal distributions. For any point $x \sim p_o(x)$, the posterior is

$$p(\theta|x) = \mathcal{N}\left(\theta; \frac{\sigma^2}{\sigma^2 + 1}x, \frac{\sigma^2}{\sigma^2 + 1}\right). \quad (14)$$

Therefore, the average posterior distribution is

$$\begin{aligned} G(\theta) &= \int \mathcal{N}\left(\theta; \frac{\sigma^2}{\sigma^2 + 1}x, \frac{\sigma^2}{\sigma^2 + 1}\right) \mathcal{N}(x; 0, \sigma_D^2) dx \\ &= \mathcal{N}\left(\theta; 0, \frac{\sigma^2}{\sigma^2 + 1} \left[1 + \frac{\sigma_D^2 \sigma^2}{\sigma^2 + 1}\right]\right). \end{aligned} \quad (15)$$

Finally, the pushforward distribution of $G(\theta)$ is

$$\begin{aligned} G^\#(x) &= \int \mathcal{N}(x; \theta, 1^2) \mathcal{N}\left(\theta; 0, \frac{\sigma^2}{\sigma^2 + 1} \left[1 + \frac{\sigma_D^2 \sigma^2}{\sigma^2 + 1}\right]\right) d\theta \\ &= \mathcal{N}\left(x; 0, 1 + \frac{\sigma^2}{\sigma^2 + 1} \left[1 + \frac{\sigma_D^2 \sigma^2}{\sigma^2 + 1}\right]\right). \end{aligned} \quad (16)$$

The variance of the pushforward distribution $G^\#(x)$ is different to the variance of the data distribution $p_o(x)$, and thus the average posterior distribution is not a valid source distribution.

A.7. Details on source estimation for the single-compartment Hodgkin-Huxley model

We use the simulators as described in [Bernaerts et al. \(2023\)](#) for our source estimation. This work provides a uniform prior over a specified box domain, which we use as the reference distribution for source estimation. Since the simulator parameters live on different orders of magnitude, we transform the original m -dimensional box domain to the $[-1, 1]^m$ cube. Note that this transformation does not affect the maximum entropy source distribution. This is because this scaling results in a constant term added to the differential entropy. More specifically, for a random variable X (associated with its probability density $p(x)$), the differential entropy of X scaled by a (diagonal) scaling matrix D and shifted by a vector c is given by

$$H(DX + c) = H(X) + \log(\det D). \quad (17)$$

The surrogate is trained on one million parameter-simulation pairs produced by sampling parameters from the uniform distribution and simulating with the sampled parameters. We do not use the simulated traces directly, but instead compute 5 commonly used summary statistics ([Bernaerts et al., 2023](#); [Gonçalves et al., 2020](#)). These are the number of spikes k transformed by a $\log(k + 3)$ transformation (ensuring it is defined in the case of $k = 0$), the mean of the resting potential, and the first three moments (mean, variance, and skewness) of the voltage during the stimulation.

As our surrogate, we choose a deterministic multi-layer perceptron, because we found that the internal noise has almost no noticeable effect on the summary statistics, so that the likelihood $p(x|\theta)$ is essentially a point function. We are able to make this choice because the sample based nature of our source distribution estimation approach is less sensitive to sharp likelihood functions, whereas likelihood-based approaches could struggle with such problems.

The multi-layer perceptron surrogate has 3 layers with a hidden dimension of 256. ReLU activations and batch normalization were used. Training of the MLP was done with Adam (learning rate $5 \cdot 10^{-4}$, weight decay 10^{-5} , training batch size 4096). Again, 20% of the data were used for validation.

A.8. Supplementary figures

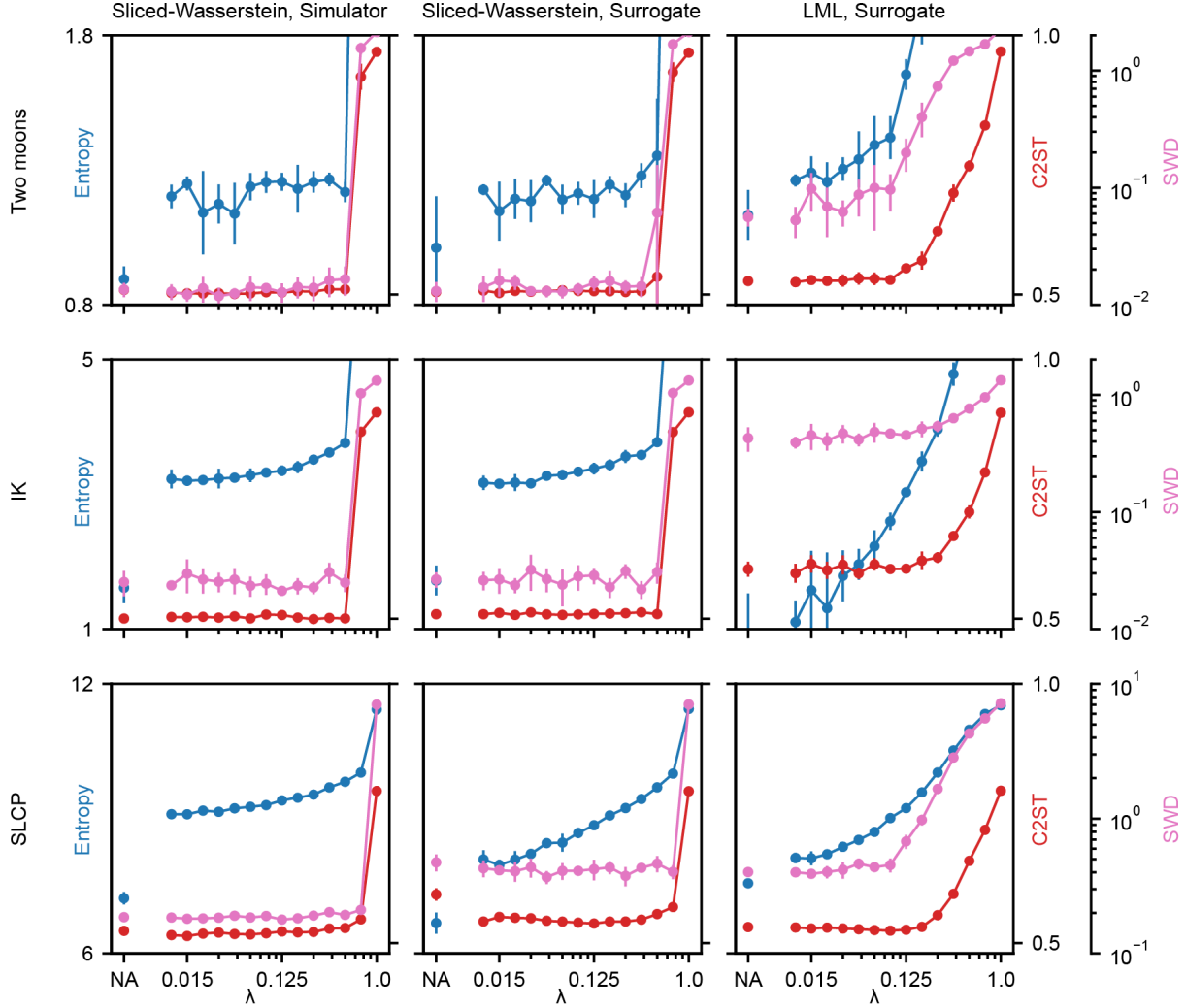


Figure 8. Extended results for source distribution estimation on the benchmark tasks (Fig. 3). The Sliced-Wasserstein distance (SWD) between the observations and the pushforward distribution of the estimated source is also shown for the two columns of Fig. 3. We also show the results of maximizing the log-marginal likelihood (LML) with a negative entropy regularization of varying strength λ . We see that for the IK task, the LML approach typically achieves a slightly worse C2ST accuracy than the SWD-based approach. Unsurprisingly, this is more noticeable when comparing the performance in terms of SWD, as this is not included in the objective function for the LML approach.

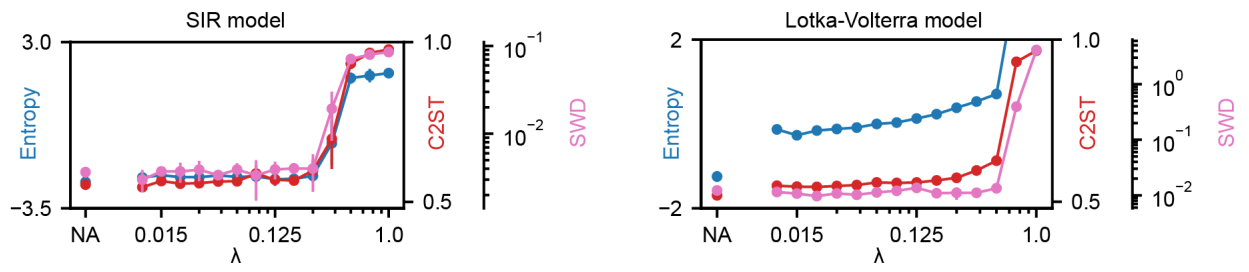


Figure 9. Extended results for source distribution estimation on the differentiable SIR and Lotka-Volterra models (Fig. 5 and Fig. 6). In addition to the Sliced-Wasserstein distance (SWD), the C2ST accuracy between the observations and the pushforward distribution of the estimated sources is shown. Despite the high-dimensional data space of the simulators (50 and 100 dimensions), the estimated sources achieve a good C2ST accuracy (below 60%) for various choices of λ .

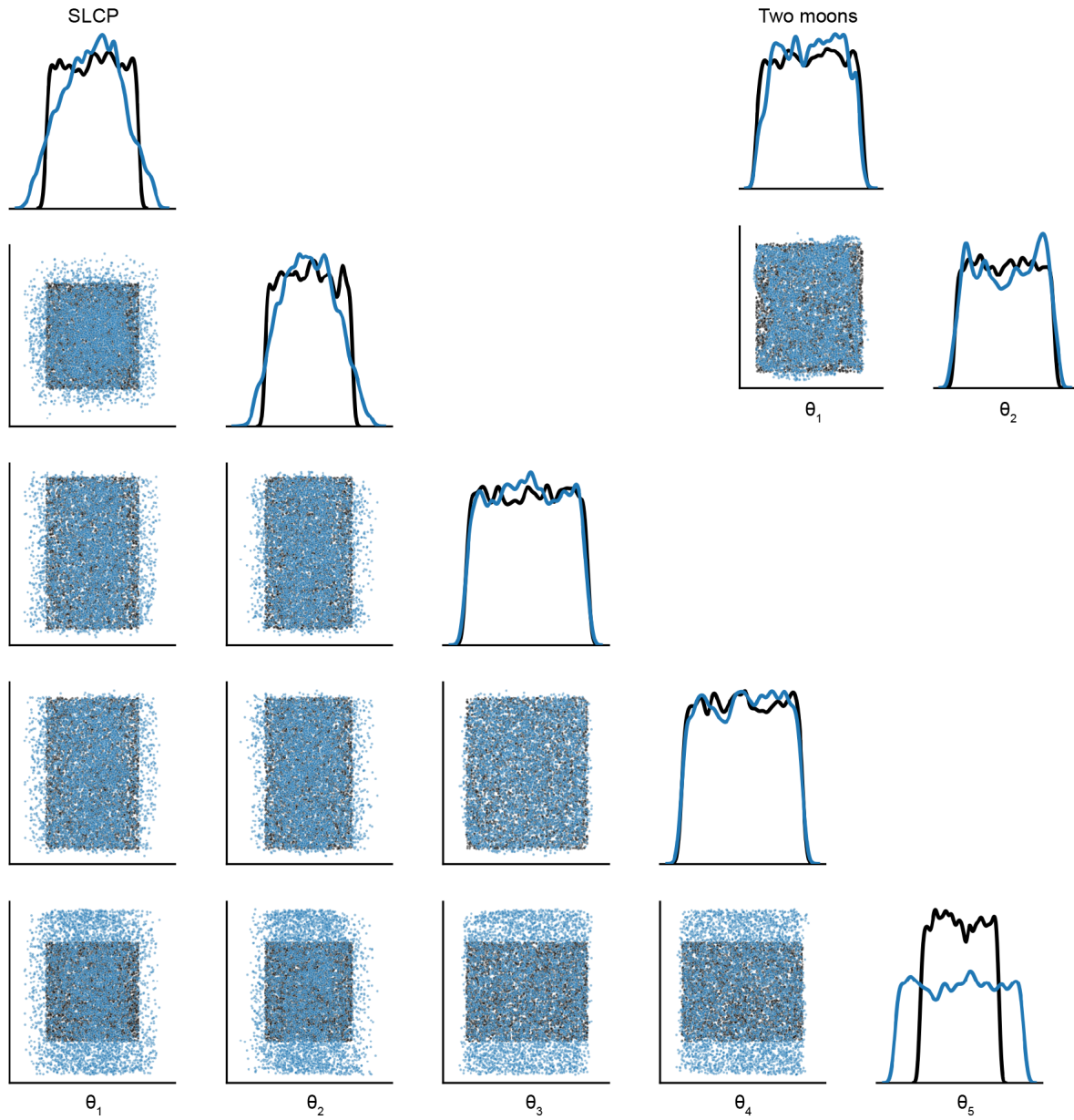


Figure 10. Original and estimated source distributions for the benchmark two moons and SLCP simulator ($\lambda = 0.35$ in both cases). For the SLCP simulator, the estimated source has higher entropy than the original source.

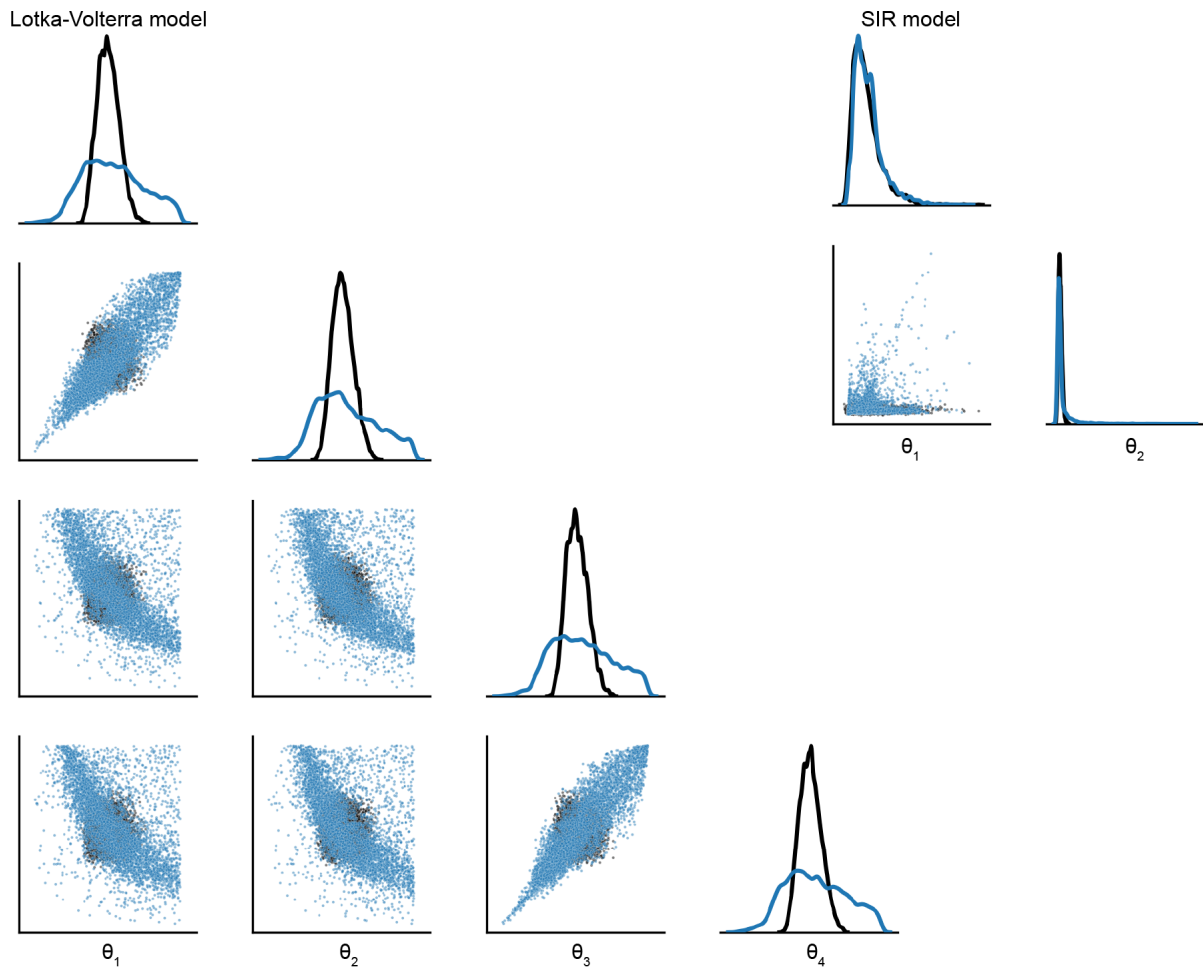


Figure 11. Original and estimated source distributions for the SIR ($\lambda = 0.25$) and Lotka-Volterra ($\lambda = 0.5$) model. For the Lotka-Volterra model, the estimated source has higher entropy than the original source.

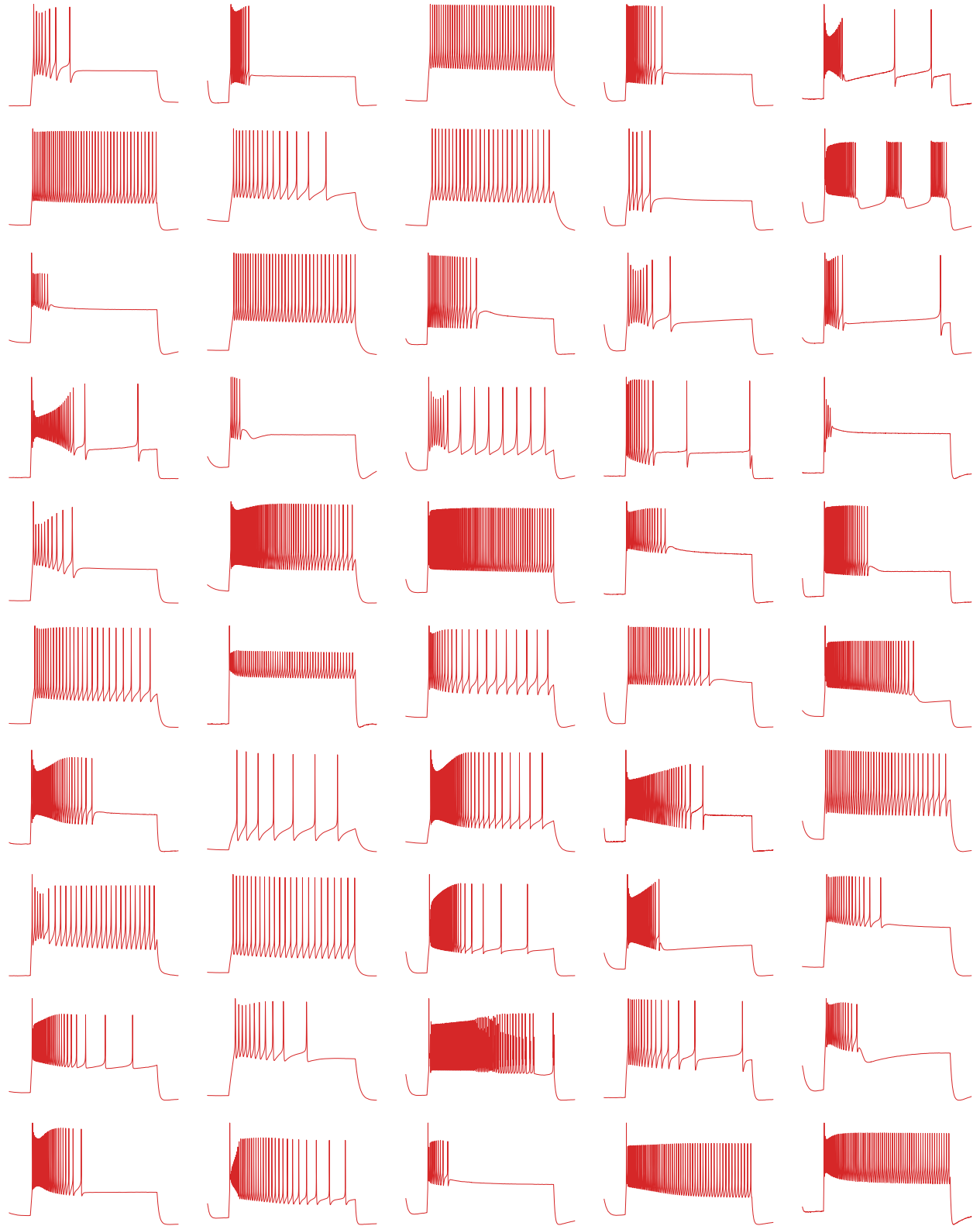


Figure 12. 50 random example traces produced by sampling from the estimated source ($\lambda = 0.25$) and simulating with the Hodgkin-Huxley model.

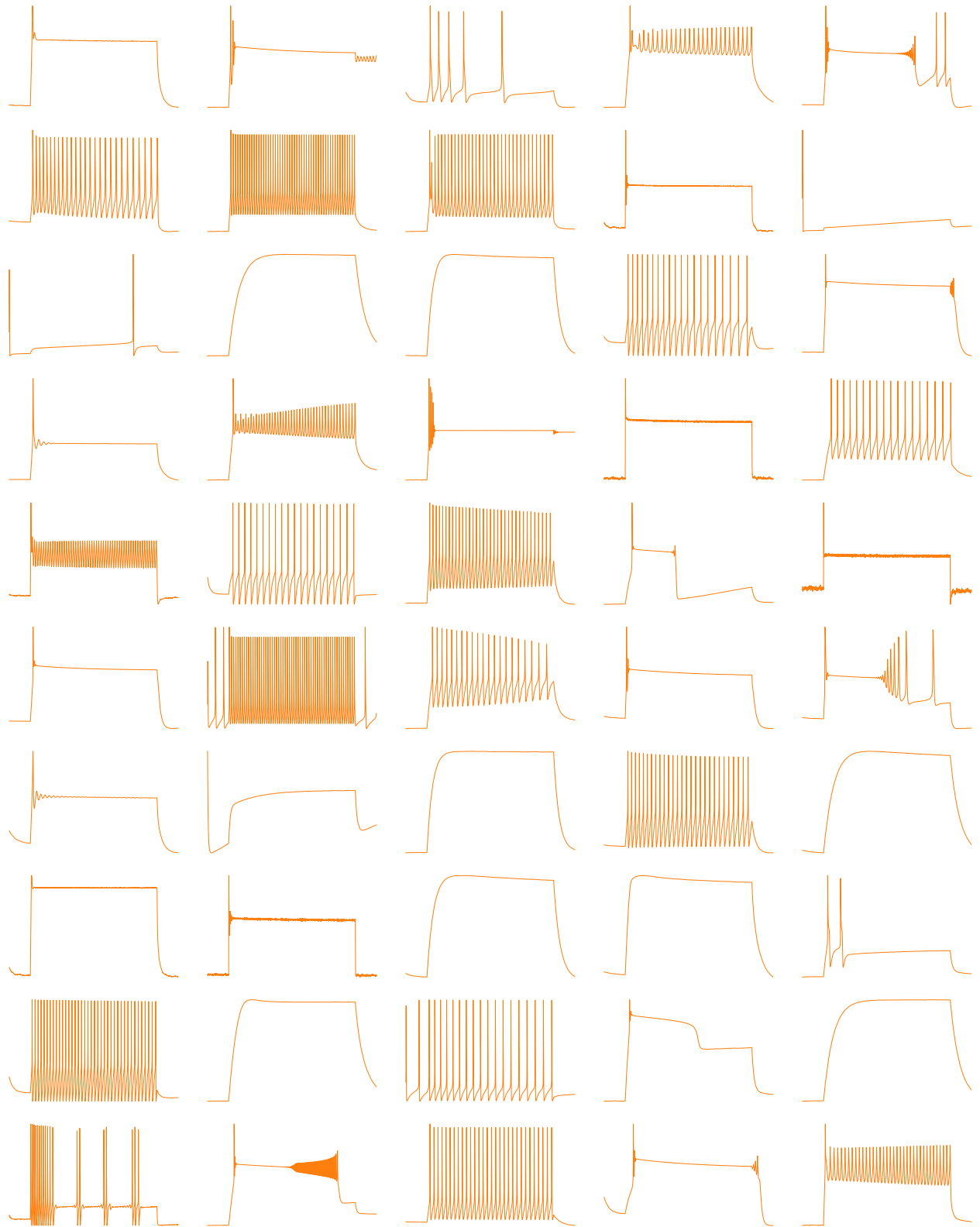


Figure 13. 50 random example traces produced by sampling from the uniform distribution over the box domain and simulating with the Hodgkin-Huxley model.

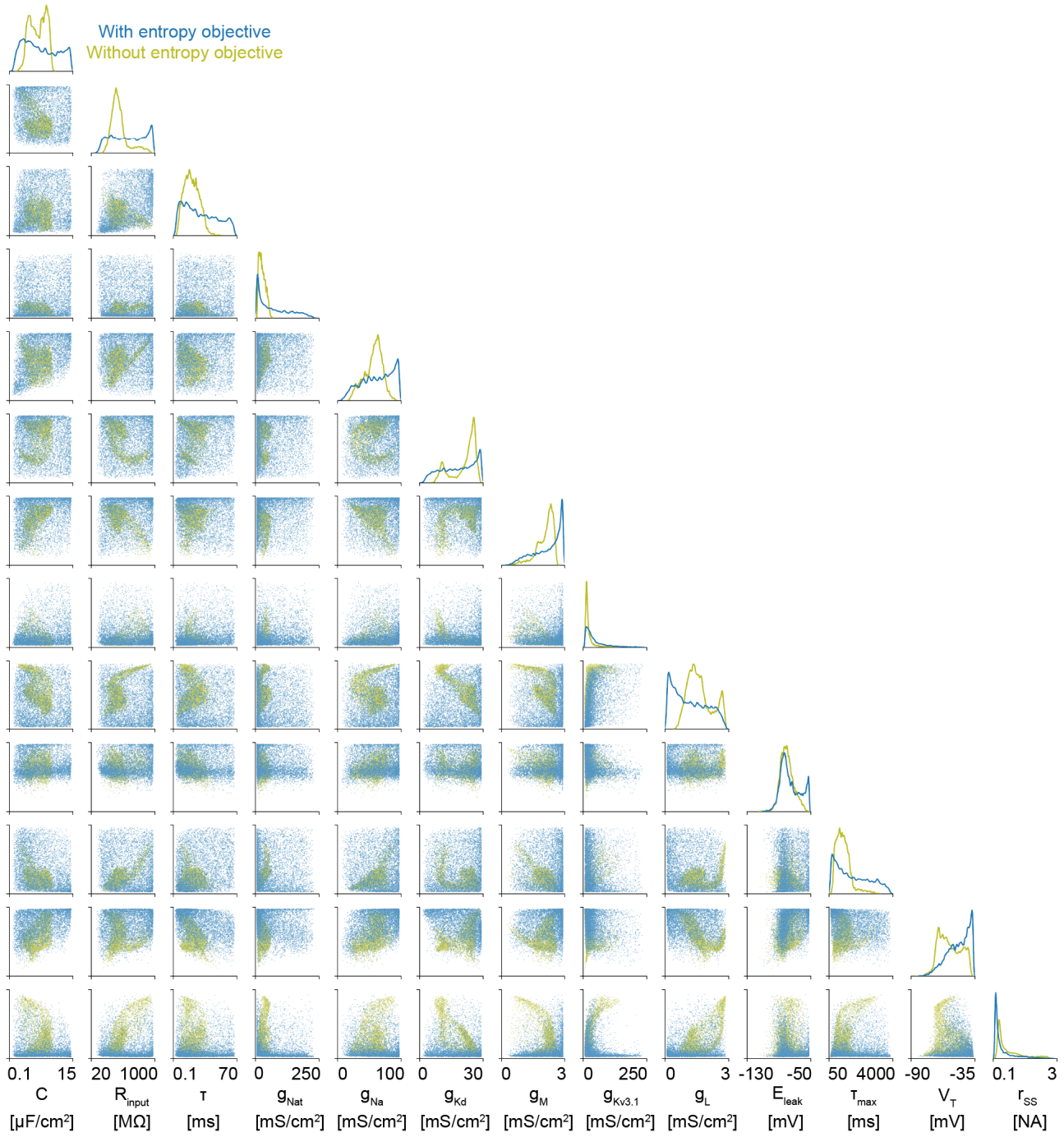


Figure 14. Estimated sources using for Hodgkin-Huxley task with the entropy objective ($\lambda = 0.25$) and without the entropy objective. Without the entropy objective, many viable parameter settings are missed, which would have significant downstream effects if the learned source distribution is used as a prior distribution for inference tasks.